Available online at www.sciencedirect.com
ScienceDirect
Journal of Sound and Vibration 318 (2008) 279–295
JOURNAL OF SOUND AND VIBRATION
www.elsevier.com/locate/jsvi

An insight into the breathing mechanism of a crack in a rotating shaft

S.K. Georgantzinos, N.K. Anifantis*

Machine Design Laboratory, Mechanical and Aeronautics Engineering Department, University of Patras, Patras GR-26500, Greece

Received 12 November 2007; received in revised form 29 February 2008; accepted 8 April 2008
Handling Editor: C.L. Morfey
Available online 19 May 2008

Abstract

The time history of local flexibilities associated with a breathing crack in a rotating shaft is the concern of this paper. Considering quasi-static approximation, the deflections of a circular cross-section beam presenting a crack of different depths, due to bending or torsion loads are analyzed with the aid of a refined nonlinear contact-finite element procedure in order to predict accurately the time-variant flexibility of the fractured shaft. This method predicts the partial contact of crack surfaces, and it is appropriate to evaluate the instantaneous crack flexibilities. The bending load is applied in several aperture angles, in order to simulate a rotating load on a fixed beam. Results obtained for the rotating beam can then be used for the analysis of cracked, horizontal axis rotors. The effect of friction is also considered in the cracked area. Portions of crack surfaces in contact are predicted, the direct and the cross-coupled flexibility coefficients are calculated by applying energy principles. The numerical results compared with relevant previously published results, show high consistency.

1. Introduction

Shafts are amongst components subjected to perhaps the most arduous working conditions in high-performance rotating equipment used in process and utility plants. Although usually quite robust and well designed, shafts in operation are sometimes susceptible to serious defects that develop without much apparent warning. They are prime candidates for fatigue cracks because of the rapidly fluctuating nature of stresses, the presence of numerous stress raisers and possible design or manufacturing flaws. The growth of cracks in the rotating components can cause severe accidents if undetected. The earlier the time of crack detection, the smaller the effort, and expenses for repair. Cracks that always remain open are known as gaping cracks. They operate like notches, are easy to mimic in a laboratory environment, and hence most experimental work is focused on this particular type of cracks. If a cracked shaft rotates under the external loading, then the crack opens and closes regularly per revolution: it breathes. The breathing mechanism is produced by the stress distribution around the crack mainly due to the action of bending moment, while the effect of torsion is

*Corresponding author. Tel.: +30 2610 997 195; fax: +30 2610 997 207.
E-mail address: nanif@mech.upatras.gr (N.K. Anifantis).

0022-460X/$ - see front matter © 2008 Elsevier Ltd. All rights reserved.
doi:10.1016/j.jsv.2008.04.010

negligible. Usually, shaft cracks breathe when crack sizes are small, running speeds are low and radial forces are large. However, there is a lack of fundamental understanding about certain aspects of the crack breathing mechanism. This involves not only the identification of variables affecting the crack breathing behavior, but also the issues for evaluating fractured rotor dynamic response. It is also not yet entirely clear how partial closure interacts with key variables of the problem. Obviously, the actual physical situation requires a model that accounts for the crack breathing mechanism and for the interaction between external loading and dynamic crack behavior. When crack contact occurs, the unknowns are the field singular behavior, the contact region, and distribution of contact tractions on the closed region of the crack. The latter class of unknowns does not exist in the case without crack closure. This type of complicated deformation of crack surfaces constitutes a nonlinear problem difficult to be treated through classical analytical procedures. A suitable numerical implementation for unknowns of the problem is thus required when partial crack closure occurs.

A crack introduces local flexibilities in the stiffness of the structure due to strain energy concentration. Although local flexibilities representing the fracture in stationary structures are constant for open cracks, the breathing mechanism causes their time dependence. In a fixed direction, local flexibilities of rotating shafts change also with time due to the breathing mechanism. Evidently, the vibrational response of a rotating shaft depends on the crack opening and closing pattern in one cycle. For the analysis of fractured shafts, the technical literature proposes several models to quantify local effects introduced by the crack. According to the simplest model, a hinge substitutes the crack and a local flexibility matrix describes the discontinuity conditions enforced by the crack presence. The coefficients of the local flexibility matrix can be calculated experimentally, as long as they depend on fracture severity and loading mode [1–4]. However, most of the experimental results are obtained with a notched shaft (gaping crack case) rather than a cracked shaft due to the difficultness of production of a geometrically controllable real crack in the laboratory. The hinge model is mostly appropriate for one-dimensional (1D) approaches in analyzing dynamic problems of fractured shafts [5–8]. In turn, local flexibilities can be calculated analytically or numerically for various loading cases, according to the strain energy release rate (SERR) approach, under the linear elastic fracture mechanics regime [9–13]. Crack geometry limitations of this approach clearly appear. The crack front must be straight, and some physical stress intensity factors are not supported. For example, the stress intensity factor of opening fracture mode tends to null value on the closed crack surface. An advanced approach in analyzing the behavior of fractured structures is the substitution of the crack by a cracked element that embodies the discontinuities imposed by the fracture and it is convenient for the application of finite element procedures [14–16].

The inherent nonlinearity implied by the crack breathing mechanism demands for the development of more sophisticated models. Among these, the switching crack model approximates the crack opening and closure mechanism by a periodic switching function [17–19]. This model is very stiff and sometimes yields erroneous structural responses. A better approximation represents the time variation of local flexibilities by an appropriate Fourier cosine expansion of the switching function [20–22]. These models utilize the SERR approach for the calculation of local flexibilities, and presume the fraction of crack-surface closure for the prediction of time dependency. The semi-analytical character of these approximations makes them to be attractive approaches of the problem. However, they are rough estimations due to the inherent weakness of them being unknown the contact area between the crack surfaces, when the crack lies in arbitrary angular position with respect to the longitudinal axis of the shaft and thus it is made a guess. An accurate model of the breathing of crack demands application of full contact conditions between the crack surfaces. Three-dimensional (3D) finite element analysis appears to hold special promise as an investigative tool for the study of crack breathing mechanism. It should simultaneously involve the deformation of a loaded shaft, the crack discontinuity, and the crack-surface interference. This method has been employed extensively in fracture mechanics to model the stress singularity at the crack tip, which is always a major consideration and has to be evaluated. One approach is to utilize singular elements. Among those, the quarter-point element has found considerable popularity because of its accuracy and simplicity [23,24].

A brief search on the relevant literature reveals that, most scientific effort has been focused on the prediction of fractured rotor dynamics rather than on the accurate simulation of the fracture itself. Recently, Bachschmid and Tanzi [12] have looked at the straight front crack and there are numerical and experimental results for the benchmark and comparison of the present work. Therefore, the exact time dependency of the crack breathing

mechanism and its relationship with the aperture angle is yet partially unresolved. The aim of this work is to study the effect of the crack breathing mechanism on the time-variant flexibility due to the crack in a rotating shaft considering quasi-static approximation. The deflections of a circular cross-section cantilever beam presenting a crack of different depths, due to bending or torsion loads are analyzed with the aid of an advanced nonlinear contact-FEM procedure in order to predict accurately the time-variant flexibility of a fractured shaft. This method predicts the partial contact of crack surfaces, and it is appropriate to evaluate the instantaneous crack flexibilities. The bending load is applied in several aperture angles, in order to simulate a rotating load on a fixed beam. Results obtained for the rotating beam can then be used for the analysis of cracked, horizontal axis rotors. The effect of friction is also considered in the cracked area. Portions of crack surfaces in contact are predicted, and the direct and the cross-coupled flexibility coefficients are calculated by applying energy principles. For reasons of accuracy, the present numerical results are compared with relevant previously published results.

2. Cracked shaft model

In this article, the deflections of a circular cross-section beam presenting a surface crack of different depths, due to bending or twisting moments, are analyzed with the aid of a rather refined 3D model, which takes into account the nonlinear contact constraints in the cracked area. Reasons of simplicity and reduction of the computational effort impose quasi-static approximation of the response of the cracked structure. Without any restriction on the generality and the applicability of the method, the shaft model chosen in the present analysis has the form of a weightless cantilever beam with uniform cross-section (Fig. 1a). The beam has length $2L$ and circular cross-section of radius R. At the middle of this beam, a crack presents with straight or curved front. The curved front has radius of curvature R, while the maximum depth of the crack is α (Figs. 1b and c). In order to study the effect of crack slope on the local flexibilities, the general case of a slant crack is considered that forms θ_y, θ_z angles with respect to (x, y) and (x, z) planes, respectively.

The morphology of the proposed models is designed in such a way that allows for changes in crack geometry. Thus, considering the crack depth and its angle as global design variables, parametric studies are possible. This is accomplished by setting the crack orientation angles θ_y, θ_z, and the crack depth α as global design variables. Thus the proposed formulation can treat several geometric models by changing the values of these parameters. The inherent nonlinearities and the model geometric attributes demand for 3D FEM approximation of the problem. An appropriate regenerative meshing scheme is developed to account for the variety of models involved in the analysis. In the vicinity of the crack region, a mesh refinement is adopted, while the crack surfaces are constrained with appropriate contact conditions. Typical finite element meshes utilized in the analysis are illustrated in Fig. 2. The number of elements and nodes for each model type are presented in Table 1. The left end of the beam is considered to be clamped, i.e. all degrees of freedom of every node that corresponds to the left end are fixed. Two different load cases are separately applied at the tip of the cantilever beam, i.e., twisting moment T and bending moment M, respectively. The bending moment is applied in several aperture angles $M = M(\varphi)$, in order to simulate a rotating load on a fixed beam. The components $M_y = M_y(\varphi)$, and $M_z = M_z(\varphi)$ of the bending moment $M(\varphi)$, along the directions of axes y and z, respectively, are functions of the aperture angle. Thus, this angle represents a third global variable of the problem.

3. Contact of crack surfaces

The crack-surface interference problem is treated in this work like a classical 3D contact between deformable but interconnected bodies at the crack front. In order to approach frictional contact between these sub-bodies, it is assumed that possible sliding obeys Coulomb's law of friction and that penetration between contacting areas is not allowed. Since the frictional contact problems are inherently nonlinear and irreversible, an incremental approach should be implemented. Primarily, the technique of obtaining the incremental finite element equations for the general problem depicted in Fig. 1 is clarified. This well-known technique is briefly reproduced here for reasons of completeness. Boldface symbols denote vectors and matrices, the order of which is indicated by the context.

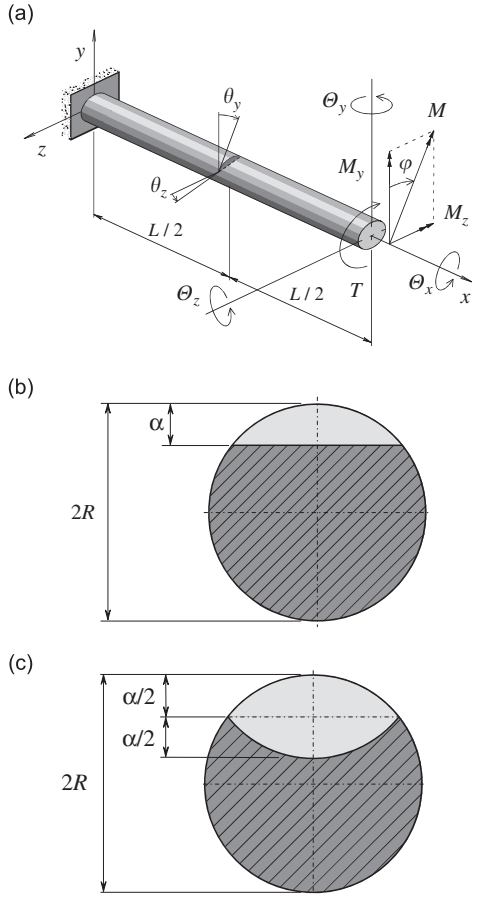

Fig. 1. The geometry of the model: (a) cracked shaft subjected to bending and twisting moments, (b) straight-front crack, and (c) curved front crack.

The discretized nonlinear system of equations can be written as a set of algebraic equations in the form

$$[\mathbf{K}_T(\mathbf{U})]\{\mathbf{U}\} = \{\mathbf{F}\} \tag{1}$$

In Eq. (1), $\{\mathbf{F}\}$ is the external force vector and $\{\mathbf{U}\}$ is the structural displacement vector, respectively. The 3D problem considered here demands for three degrees of freedom per node. If N nodes in total describe the discretized shaft FEM model, then the dimension of the above vectors is $3N$, and that of the matrix $3N \times 3N$. Both are generally zero at the start of the problem. To trace the nonlinear structural response, a load stepping procedure must be used. Assuming that the load is applied in M equal small increments of the form $\{\Delta\mathbf{F}^m\} = \{\mathbf{F}^m\} - \{\mathbf{F}^{m-1}\}$, $m = 1, 2, \ldots, M$, an incremental procedure is then set up. The incremental procedure makes use of the fact that the solution for $\{\mathbf{U}^{m-1}\}$ is known when the load term $\{\mathbf{F}^{m-1}\}$ is applied to the structure. Such a method can yield reasonable results and guaranteed to converge if a suitably small increment of $\{\mathbf{F}\}$ is chosen.

The application of a trial load $\{\Delta\mathbf{F}^m\}$ at the step m of the procedure yields the incremental form of Eq. (1) in the form

$$[\mathbf{K}_T]\{\Delta\mathbf{U}^m\} = \{\Delta\mathbf{F}^m\} \tag{2}$$

where $[\mathbf{K}_T]$ is the tangent stiffness matrix, and $\{\Delta\mathbf{U}^m\} = \{\mathbf{U}^m\} - \{\mathbf{U}^{m-1}\}$ is the increment in the structural displacement. At any increment m must be satisfied also the equilibrium condition

$$\{\mathbf{R}^m\} = \{\mathbf{P}^m\} - \{\mathbf{F}^m\} \approx \{\mathbf{0}\} \tag{3}$$

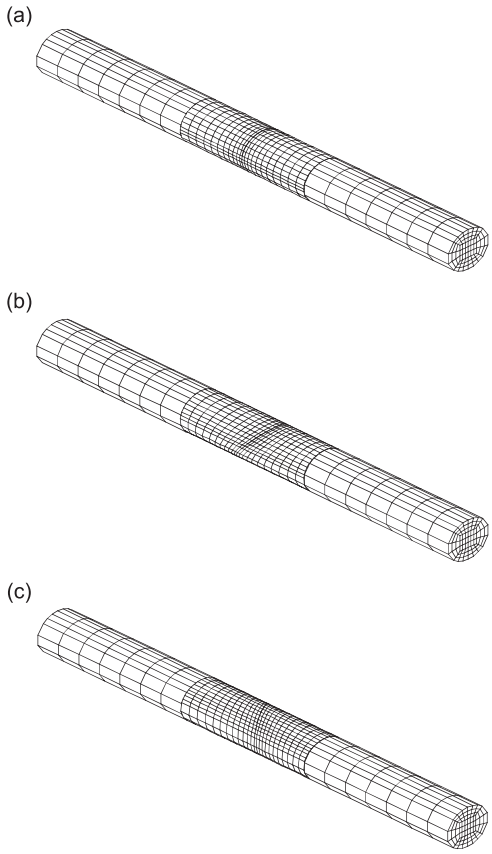

Fig. 2. Typical finite element meshes: (a) transverse crack with depth $a/R = 0.4$, (b) slant crack with respect to y-axis ($\theta_y = 45^\circ$, $a/R = 0.6$) and (c) slant crack with respect to z-axis plane ($\theta_z = 30^\circ$, $a/R = 0.8$).

Table 1
Modeling size information

Model type	Crack depth (a/R)	Number of elements	Number of nodes
Straight front crack	0.2	4620	4980
	0.4	4380	4712
	0.6	4140	4736
	0.8	4140	4444
Curved front crack	0.2	5004	5344
	0.4	5004	5344
	0.6	4716	5022
	0.8	4716	5024

where $\{\mathbf{R}^m\}$ is the residual, and $\{\mathbf{P}^m\}$ is the vector of internal forces. The solution of the problem posed by Eqs. (2) and (3) cannot approach directly and some form of iteration will be always required to zero the residual and restore the equilibrium for every load step. The iterative procedure approximately achieves the solution and some tolerance limits are set to terminate the iteration and ensure the convergence of the iterative procedure [25].

The crack is constituted from the surfaces ${}^{\mathrm{I}}S$ and ${}^{\mathrm{II}}S$ which intersect on the crack front and may come to contact on an interface ${}^{c}S$, given by ${}^{c}S = {}^{\mathrm{I}}S \cap {}^{\mathrm{II}}S$. The size of ${}^{c}S$ can vary during the interaction between the load and the structure, but usually constitutes from two parts, i.e., an adhesive (${}^{a}S$), and a slipping (${}^{s}S$) one, depending on the friction conditions maintained between the contacting surfaces. In the open crack state, the ${}^{o}S$ part of the crack surface subjects to traction-free condition.

The crack surfaces are defined by the local coordinate systems $({}^{j}x_1, {}^{j}x_2, {}^{j}x_3)$, $j = \mathrm{I}, \mathrm{II}$. Both the axes ${}^{j}x_3$ define the direction of the unit outward normal vector of the corresponding surfaces. The so-called slave–master concept that is widely used for the implementation of contact analysis is adopted in this work for prediction of the crack-surface interference. Assuming that the crack surface ${}^{\mathrm{I}}S$, is the slave, the nodes on this surface are called slave nodes. Then the surface ${}^{\mathrm{II}}S$ is the master one and the nodes that belong to this are called master nodes. Contact segments that span master nodes cover the contact surface of the structure. Therefore, the above problem can be regarded as contact between a slave node and a point on a master segment. This point may be located at a node, an edge, or a point of a master segment. A slave node makes contact with only one point on the master segments, but one master segment can make contact with one or more slave nodes at each time. For every contact pair, the mechanical contact conditions are expressed in a local coordinate system in the direction of the average normal to the boundaries of the bodies. Lowercase symbols ${}^{j}u_i^m$ and ${}^{j}f_i^m$, $i = 1, 2, 3$ denote nodal displacement and force components, respectively, defined on the local coordinate systems $({}^{j}x_1, {}^{j}x_2, {}^{j}x_3)$, $j = \mathrm{I}, \mathrm{II}$. For reasons of simplicity, the subscripts that indicate nodal numbers were dropped out.

Recalling the equilibrium condition, between the components of the incremental force are always maintained by the following equations

$$ {}^{\mathrm{I}}\Delta f_i^m + {}^{\mathrm{II}}\Delta f_i^m = 0, \quad i = 1, 2, 3 \tag{4} $$

In the open crack state (surface ${}^{o}S$), the incremental traction components are simplified as follows:

$$ {}^{\mathrm{I}}\Delta f_i^m = -{}^{\mathrm{II}}f_i^{m-1}, \quad i = 1, 2, 3 \tag{5} $$

By the definition of adhesion, on the corresponding crack surfaces (${}^{a}S$), the incremental displacement components are interconnected by the equation

$$ {}^{\mathrm{I}}u_i^{m-1} + {}^{\mathrm{I}}\Delta u_i^m = {}^{\mathrm{II}}u_i^{m-1} + {}^{\mathrm{II}}\Delta u_i^m, \quad i = 1, 2 \tag{6} $$

When exists a gap g^0 in the normal direction, then the incremental displacement component along the normal direction is

$$ {}^{\mathrm{I}}u_3^{m-1} + {}^{\mathrm{I}}\Delta u_3^m = {}^{\mathrm{II}}u_3^{m-1} + {}^{\mathrm{II}}\Delta u_3^m - g^0 \tag{7} $$

where g^0 is the initial normal gap between the master and slave node of the corresponding node-pair. The slip state does not prohibit the existence of a gap between the crack surfaces, so Eq. (7) is still valid in this case. However, the coplanar force components are defined in terms of friction

$$ {}^{\mathrm{I}}f_i^{m-1} + {}^{\mathrm{I}}\Delta f_i^m = \pm\mu({}^{\mathrm{I}}f_3^{m-1} + {}^{\mathrm{I}}\Delta f_3^m), \quad i = 1, 2 \tag{8} $$

where μ is the coefficient of Coulomb friction.

The constraints appearing in Eqs. (4)–(8) can be embedded in the previously reported incremental FEM procedure if are transformed to the global coordinate system and properly assembled to the master system of Eq. (2). Assume that the problem has been solved for the step $m-1$ and consequently that the total nodal values $\{\mathbf{U}^{m-1}\}$, $\{\mathbf{F}^{m-1}\}$ are known for the whole structure. To determine the corresponding total nodal values of the step m, the contact conditions must be satisfied first. Therefore, the iterative procedure must be applied by initially utilizing the convergent contact status $c = a \cup s \cup o$ of the previous step $m-1$. The procedure initially assumes that ${}^{\mathrm{I}}\Delta f_i^m = 0$, $i = 1, 2, 3$. Then, the accurate values of incremental forces can be estimated via the iterative procedure. The contact state for every node-pair is examined according to Table 2. This table describes criteria to check if violations involving geometrical compatibility and force continuity have occurred. Where necessary, appropriate changes from open to contact and from adhesion to slip state, and vise versa are made to seek the equilibrium state of contact conditions. For the node-pair closest to a change, the new contact condition is applied. If the change is from open state to contact state, then the adhesion condition is adjusted. When the iterative procedure is converged, the incremental nodal values $\{\Delta\mathbf{U}^m\}$, $\{\Delta\mathbf{F}^m\}$ become

Table 2
Definition of contact status

Assumption	Decision	
	Open	Contact
Open	${}^{\mathrm{II}}\Delta u_3^m - {}^{\mathrm{I}}\Delta u_3^m > {}^{\mathrm{I}}u_3^{m-1} - {}^{\mathrm{II}}u_3^{m-1} + g^0$	${}^{\mathrm{II}}\Delta u_3^m - {}^{\mathrm{I}}\Delta u_3^m \leqslant {}^{\mathrm{I}}u_3^{m-1} - {}^{\mathrm{II}}u_3^{m-1} + g^0$
Contact	${}^{\mathrm{I}}f_3^{m-1} + {}^{\mathrm{I}}\Delta f_3^m \geqslant 0$	${}^{\mathrm{I}}f_3^{m-1} + {}^{\mathrm{I}}\Delta f_3^m < 0$
	Adhesion	Slip
Adhesion	$\lvert {}^{\mathrm{I}}f_i^{m-1} + {}^{\mathrm{I}}\Delta f_i^m \rvert < \lvert \mu({}^{\mathrm{I}}f_3^{m-1} + {}^{\mathrm{I}}\Delta f_3^m) \rvert,\ i = 1,2$	$\lvert {}^{\mathrm{I}}f_i^{m-1} + {}^{\mathrm{I}}\Delta f_i^m \rvert \geqslant \lvert \mu({}^{\mathrm{I}}f_3^{m-1} + {}^{\mathrm{I}}\Delta f_3^m) \rvert,\ i = 1,2$
Slip	$({}^{\mathrm{I}}f_i^{m-1} + {}^{\mathrm{I}}\Delta f_i^m)({}^{\mathrm{I}}\Delta f_i^m - {}^{\mathrm{II}}\Delta f_i^m) > 0,\ i = 1,2$	$({}^{\mathrm{I}}f_i^{m-1} + {}^{\mathrm{I}}\Delta f_i^m)({}^{\mathrm{I}}\Delta f_i^m - {}^{\mathrm{II}}\Delta f_i^m) \leqslant 0,\ i = 1,2$

known for the whole structure. After calculating the total nodal values the procedure goes to the next step of the load increment and continues until the final increment M is reached. Then, the solution of the problem is evidently attained.

In order to simplify the computation, interference conditions associated with partial closing and opening of the crack surfaces, were modeled through the slideline facility which is available in some commercial finite element codes. Slidelines comprised two non-regular necessarily surfaces which are defined by a number of contact segments corresponding to external faces of elements closest to the surfaces. The nodal constraint treatment allows for adjustment of contact conditions by setting appropriate constraints. At each increment of the procedure, this facility tracks the node pairs being nearly in contact, and adjusts the contact constraints. This technique does not directly couples nodal degrees of freedom but introduces repellent forces between the penetrating regions of the two surfaces. Coupling of the nodal freedoms in this manner introduces no additional equations into the solution and the technique is sufficiently flexible to be implemented within both explicit and implicit type of finite element codes. Therefore, the contact status between the crack surfaces can be tracked in every step of the incremental procedure.

4. Calculation of local flexibilities

Since the torsional and bending vibrations of rotors are the most important, present analysis assumes that the corresponding local flexibilities are also dominant in the local flexibility matrix, neglecting the cross-coupling terms. Numerical results showed that the off-diagonal coefficients of this matrix are at least two orders of magnitude lower than the diagonal ones, and thus are considered negligible. Therefore, the presence of the crack can equivalently represented by a diagonal local flexibility matrix, independent of the crack contact conditions.

The exact relationship between the fracture characteristics and the induced local flexibilities is difficult to be determined by the strain energy approach, because, stress intensity factor expressions for this complex geometry are not available. For the computation of the local crack compliance, a finite element method was used. According to the point load displacement method, if at some node preferable lying on the tip of the beam is applied the external load vector $\{Q\} = \{\, T \quad M_y \quad M_z \,\}^{\mathrm{T}}$, then at the same node the resulting rotations $\{\Theta\} = \{\, \Theta_x \quad \Theta_y \quad \Theta_z \,\}^{\mathrm{T}}$ are such that

$$\begin{bmatrix} c_x & 0 & 0 \\ 0 & c_y & 0 \\ 0 & 0 & c_z \end{bmatrix} \begin{Bmatrix} T \\ M_y \\ M_z \end{Bmatrix} = \begin{Bmatrix} \Theta_x \\ \Theta_y \\ \Theta_z \end{Bmatrix} \tag{9}$$

In Eq. (9), c_r, $r = x, y, z$ are the diagonal coefficients of the local flexibility matrix. Under the application of a particular load component Q_r at the r-direction, the above equation is then simplified as follows:

$$\Theta_r = c_r Q_r \tag{10}$$

where Θ_r, $r = x, y, z$ is the induced rotation, and c_r is the local flexibility component that corresponds to the particular loading mode Q_r. Eq. (10) can be used for the computation of the local flexibility coefficients, as described in the following.

When the original uncracked beam is uploaded until the load Q_{ro}, a rotation is imposed in r-direction, such that Eq. (10) gives

$$\Theta_{ro} = c_{ro} Q_{ro} \tag{11}$$

where c_{ro} is the flexibility of the original structure. The deformation of the cracked beam when loaded at the same node gives

$$\Theta_{rc} = c_{rc} Q_{rc} \tag{12}$$

where c_{rc} is the flexibility of the cracked beam, and Q_{rc}, Θ_{rc} the applied load and the resulting rotation, respectively. Between the flexibilities of the original and the fractured structure holds the condition

$$c_{rc} = c_r + c_{ro} \tag{13}$$

where c_r is the local flexibility due to the crack itself. Assuming that the applied load levels are of the same magnitude, i.e. $Q_{rc} = Q_{ro} = Q_r$, after some manipulation, Eqs. (11)–(13) yield the local flexibility coefficient in the r-direction

$$c_r = \frac{\Theta_{rc} - \Theta_{ro}}{Q_r} \tag{14}$$

Eq. (14) is used to compute the coefficients of the local flexibility matrix $[c]$ utilizing the FEM results. Tip loads Q_r, $r = x, y, z$ are applied independently, and the resulting rotations Θ_r are evaluated. The rotations of the original structure Q_{ro}, are evaluated for FEM models that do not present crack but have similar meshing with the cracked models. When fractured models are examined, FEM results are computed for several values of the design global variables. In order to predict the contact conditions occurring between the crack surfaces, the loads are applied incrementally, though iterations yield better approximations of the solution. Therefore, the crack breathing effect is taken into account for each loading mode and aperture angle.

5. Numerical results and discussion

The previously described numerical procedure was implemented in order to reveal the crack breathing mechanism in rotating shafts subjected to torsional or bending loads. At each increment of the nonlinear procedure, a finite element analysis is performed, the contact conditions are updated to confirm with contact criteria, and the corresponding local flexibility due to the crack presence and deformation is evaluated. The closure of the crack induces additional displacements with respect to the non-cracked rotor, and thus the evaluation of the local flexibilities is achieved through Eq. (14). The presence of the crack is exclusively simulated by the uncoupled local flexibilities as described in the previous section. Among the crack breathing mechanism, the local flexibility characteristics for each particular loading mode depend on the fracture depth and orientation. In order to elucidate the performance of the previously described numerical procedure, computational results are presented, concerning the variation of the local flexibilities with the load aperture angle. For the purposes of the present study and without loss of generality, steel shafts were considered with length $L = 1.0\,\text{m}$, and radius $R = 0.05\,\text{m}$. The material properties were assumed to be $E = 210\,\text{GPa}$ for the modulus of elasticity, and $\nu = 0.3$, for Poisson's ratio, respectively. The crack surfaces are assumed to be smooth, the crack thickness is negligible, and when the shaft is under zero load conditions, then on the crack surfaces traction-free conditions occur. Parametric studies were conducted by varying the crack depth until $a = R$, and the crack orientation slopes θ_y, θ_z with respect to the global coordinate axes y and z, respectively. In order to evaluate the accuracy of the proposed models and the sensitivity of the solution to the involved parameters, an extensive number of numerical tests were conducted varying element size, mesh density crack size and geometry. The analysis shows that for double mesh density of the proposed one, there is convergence in the results for all cases, since the deviation was less than 1.5%. Numerical experimentation shows that for the smooth crack surfaces examined, the results are very little affected by the values of the coefficient of

friction. Hence, results presented in the following for a small friction coefficient ($\mu = 0.1$) should be reasonably unaffected for most of the examined cases. The local flexibility coefficients are presented in the normalized form

$$C_r = \frac{ER^3}{(1-\nu^2)} c_r, \quad r = x, y, z \tag{15}$$

For reasons of comparison, Fig. 3 depicts numerical results for the case of a gaping straight front crack, when is independently loaded in pure bending M_z, i.e. $\varphi = 90^\circ$ or twisting moment T. The application of bending moment for this transversely fractured structure imposes the bending mode local flexibility C_z

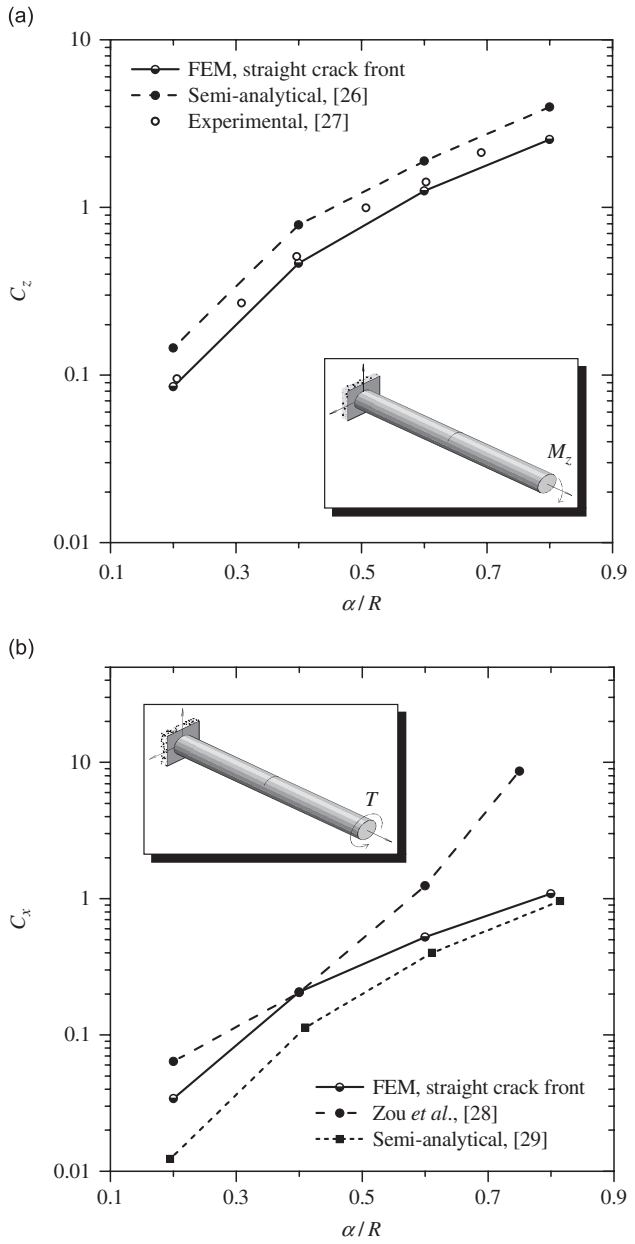

Fig. 3. Flexibility of a transverse straight front crack subjected to traction-free conditions: (a) bending flexibility coefficient C_z and (b) torsional flexibility coefficient C_x.

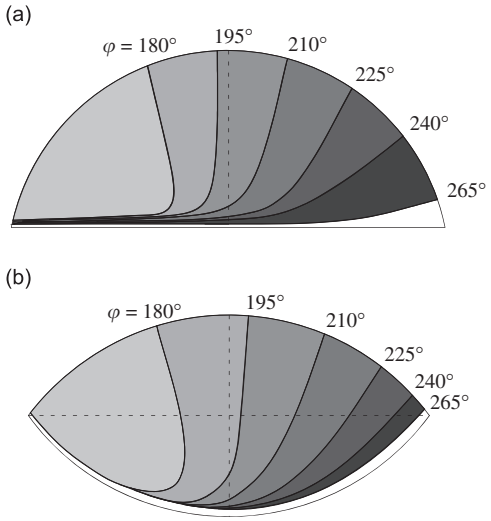

Fig. 4. Evolution of contact area between the crack surfaces for a transverse crack under bending loading: (a) straight front crack and (b) curved front crack.

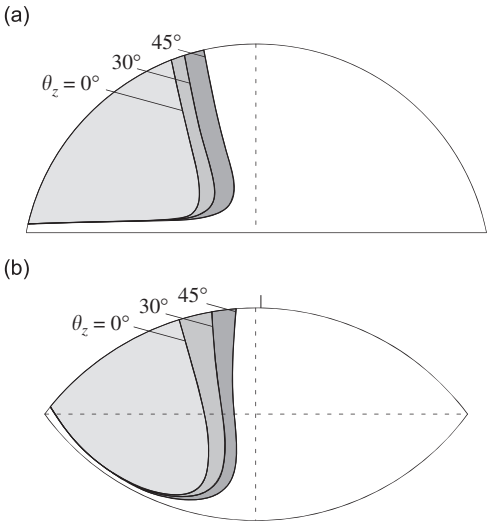

Fig. 5. Contact area between crack surfaces for different crack slopes when the shaft is loaded in bending ($\theta_y = 0$, $\varphi = 90^\circ$): (a) straight front crack and (b) curved front crack.

(Fig. 3a). When in the same fractured structure, is applied twisting moment, then only the twisting coefficient is C_x exists (Fig. 3b). Good correlation between the present results and those previously semi-analytical or experimental ones, reported in the literature [26–28] is observed. Fig. 4 illustrates predictions of the crack closure portion for a transverse crack with depth $a/R = 0.8$, when the shaft is loaded in bending moment only, versus the aperture angle. Fig. 4a shows the crack closure evolution for a straight front crack, and Fig. 4b for a curved front crack, respectively. As the aperture angle increases, the crack closure portion increases in both cases examined. On full load reversal, a very small portion of the crack surface along the crack front remains always open. The shape of the contact surface and its portion clearly depends on the shape of the crack. This fact is expected to impose differences between the local flexibilities of different crack shapes. When the crack is slant, smaller portions of the crack surfaces are in contact. Fig. 5 depicts this situation for cracks having slope θ_z with respect to the z-axis ($\theta_y = 0^\circ$), loaded in bending M_z (or $\varphi = 90^\circ$). The crack slope θ_z seems to affect slightly the size and shape of the contact area between the crack surfaces for both of the crack fronts under

investigation. The cases of crack orientation subjected to bending load that are not illustrated here present similar behavior with respect to the crack-surface contact. For cracks subjected to twisting moment, the contact area does not generally change during the shaft rotation. Fig. 6 depicts this fact when the crack slope is defined by the angles $\theta_y = 45^\circ$ and $\theta_z = 0^\circ$. Fig. 7 illustrates the dimensionless local flexibility coefficients in terms of the crack depth (a/R), when the crack slope θ_y is variable while $\theta_z = 0^\circ$. If the crack is loaded with the component M_z (or $\varphi = 90^\circ$) of the bending moment only, then the coefficient C_z exists only (Fig. 7a). Alternatively, the loading with the M_y (or $\varphi = 0^\circ$) component of bending moment alone, enforces the existence of the C_y coefficient (Fig. 7b). Fig. 8 depicts relevant numerical results in the case of a crack with variable slope θ_z while $\theta_y = 0^\circ$. Similarly, the bending component M_z (or $\varphi = 90^\circ$) enforces the existence of the coefficient C_z (Fig. 8a), while the bending component M_y enforces the existence of the coefficient C_y (Fig. 8b). As expected, local flexibility coefficients increase with the crack depth. In both cases, the curved crack front results in smaller values of the corresponding flexibilities. Although these coefficients depend on the crack depth (a/R) and the shape of the crack front, the crack slope slightly affects them. Figs. 7 and 8 illustrate extreme values of local flexibility coefficients C_z and C_y that correspond to specific limit values of the aperture angle, i.e. $\varphi = 0^\circ$ and 90°. For intermediate values, local flexibilities vary, as reported in the following. Fig. 9 shows the dimensionless coefficient C_x, when a slant crack is subjected to twisting moment T, versus the crack depth. In this case, the shape of the crack front seems to affect in a much more manner the twisting local flexibility, than the previous bending modes. As the crack is oriented with higher θ_y crack angles (Fig. 9a) the local flexibility decreases for the same crack depth due to the partial closure of crack surfaces (Fig. 6). As the θ_z crack angles increase (Fig. 9b), there is a important decrease of the local flexibility for the same crack depths because of the full closure of the crack surfaces, in contrast with the transverse case, in which the crack is fully open. Fig. 10 presents the variation of the flexibility coefficient C_y when a transversely cracked shaft is subjected to bending moment $M = M(\varphi)$. The numerical results are plotted for a period that corresponds to one revolution of the shaft. For better reasons of understanding, the local flexibility is plotted with phase lag $\pi/2$ that corresponds to the application only of the M_z component of bending moment or $\varphi = 90^\circ$. That is, the evolution of the local flexibility is progressing from the full open condition of the crack.

The same figure illustrates numerical [12], theoretical [29] and experimental [30] results from the literature for straight-fronted edge crack and crack depth $a/R = 1.0$. As it is shown, the values of local flexibility for crack depth $a/R = 1.0$, from FEM analysis are smaller than the other methods, when the crack is open. The experimental results are obtained for notched shaft which is more flexible than the cracked shaft. As the crack closes the FEM results are greater than the others. This is explained by the crack contact area (Fig. 4), which differs and is generally smaller than the area assumed by the theoretical approaches for the same edge orientation. The impossibility of these approximations to predict the crack closure correctly is the main reason

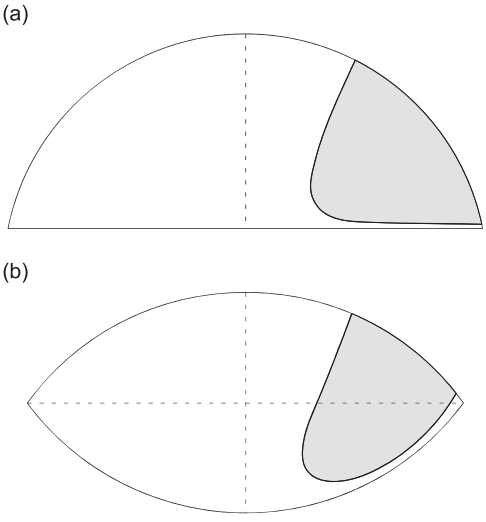

Fig. 6. Contact area between crack surfaces when the shaft is loaded in torsion: (a) straight front crack and (b) curved front crack.

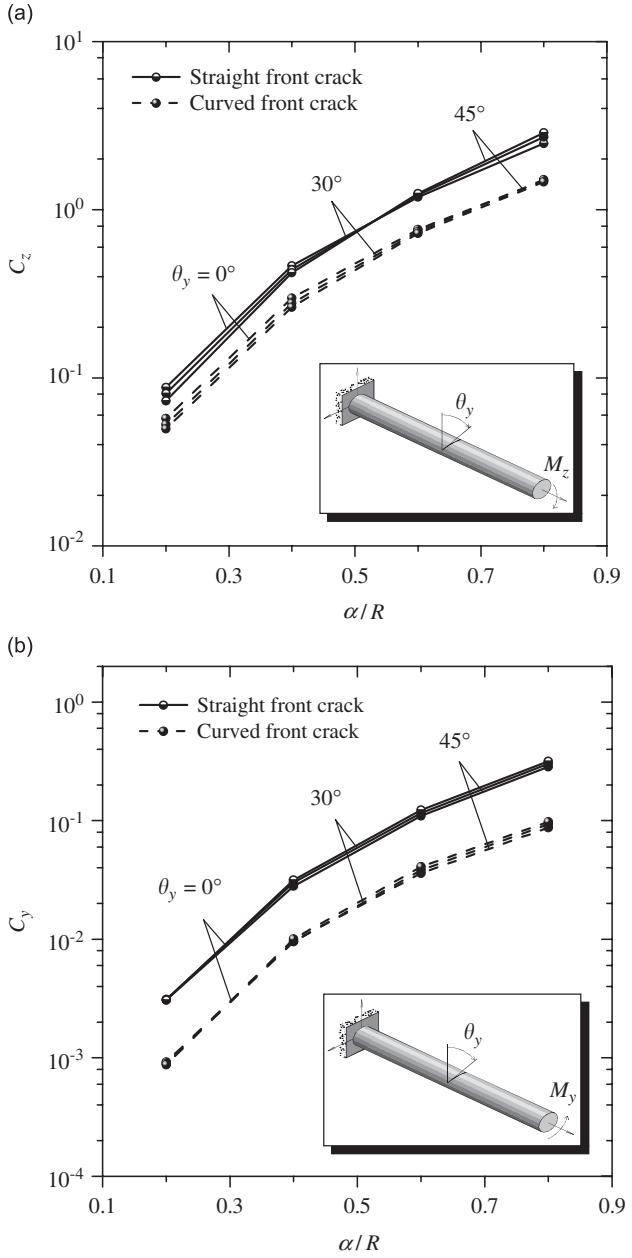

Fig. 7. Dimensionless bending compliance versus crack depth for a slant crack at different θ_y angles: (a) $\varphi = 0^\circ$ and (b) $\varphi = 180^\circ$.

that these yield comparable results with the present ones only on the regions of partially opening portion of the crack, i.e., between $0.5\pi < \varphi < \pi$ or $2\pi < \varphi < 2.5\pi$. These results show that the switching model of the crack breathing is not adequate for the modeling of the time variation of the crack breathing mechanism. Besides the impossibility of comparison of the present results to those in Ref. [31], it could be noticed that for the experimental results obtained from a rotor system that includes a beam with a realistic fatigue crack, the same trend with the corresponding results of the proposed method is observed. By the way the same trend is also shown by the data of Ref. [12] (Fig. 10(a)) and the small discrepancy yields from the difference in formulation. The variation of the coefficient C_y depends significantly on the crack depth. For small crack depths, the crack does not open regularly once per revolution, but contact is observed twice per revolution. The second contact state yields smaller compliance than the regular contact. This type of deformation of crack surfaces is

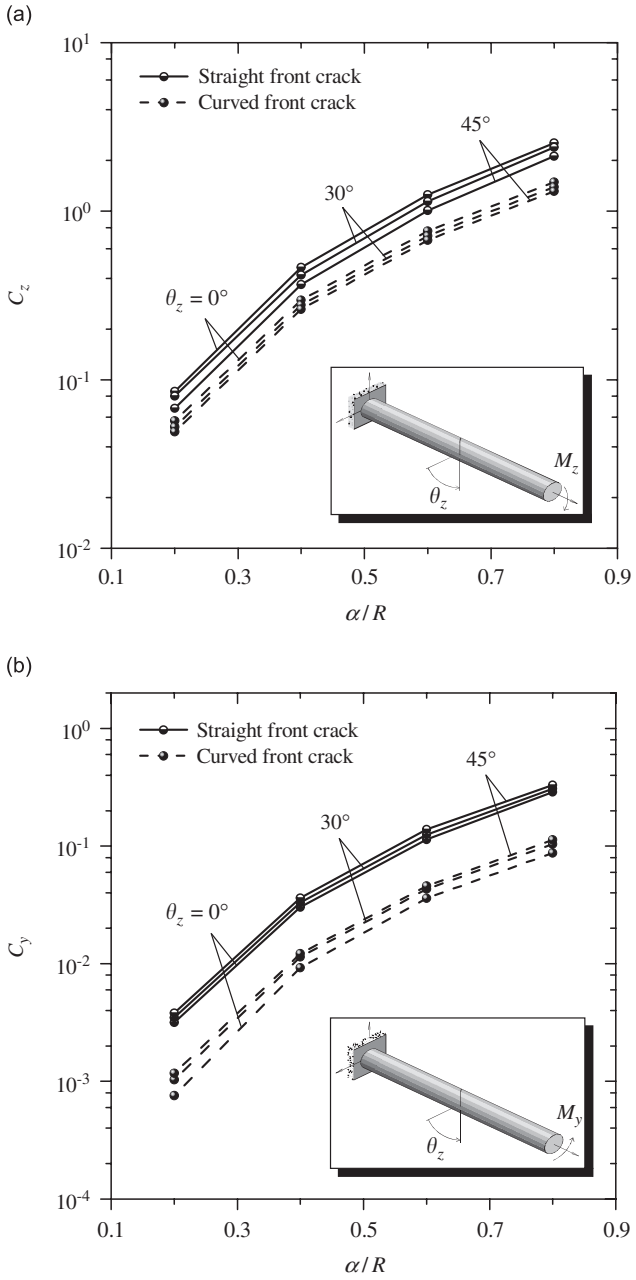

Fig. 8. Dimensionless bending compliance versus crack depth for a slant crack at different θ_z angles: (a) $\varphi = 0°$ and (b) $\varphi = 180°$.

characteristic of the crack and depends on its geometry and loading mode. Fig. 10b depicts this fact for the case of curved front transverse cracks loaded in bending. The C_y values are smaller, in this case, than the straight-fronted crack. This fact can be explained from the comparison of the areas of straight and curved front cracks which have the same depth. The portion of the crack surface being on contact is always higher for the curved front crack (Fig. 4). For this fracture case, where the crack is transverse and the shaft is loaded by the bending moment $M = M(\varphi)$ alone, reasons of symmetry indicate that $C_z = C_y$, with appropriate phase shift. Thus on the plane (x, z) the same variation of the local flexibility occurs. The effect of breathing mechanism on the local flexibility C_y, when a slant crack exists, is illustrated in Fig. 11. As previously, the shaft

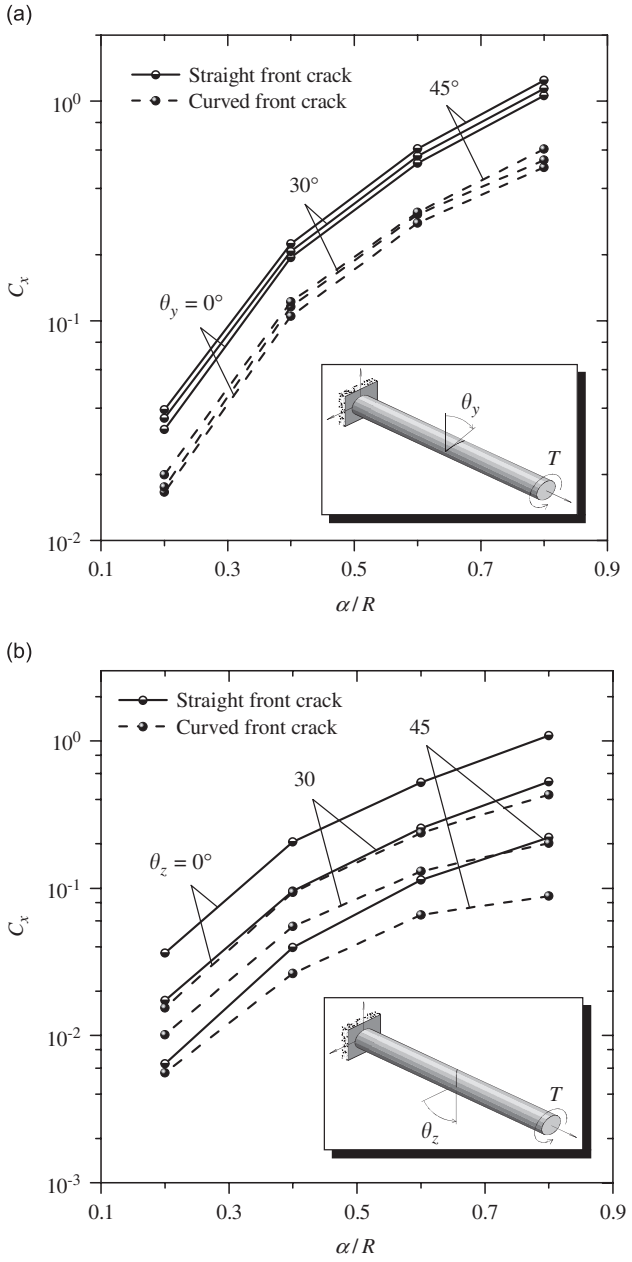

Fig. 9. Dimensionless torsional compliance C_x versus crack depth: (a) crack slope $\theta_z = 0^\circ$ and (b) crack slope $\theta_y = 0^\circ$.

is loaded at the tip by the bending moment $M = M(\varphi)$. Numerical results are plotted for fixed crack depth $a/R = 0.8$, versus the crack slope. Fig. 11 depicts the case where $\theta_z = 0$ for various values of the slope angle θ_y. If the crack forms angle $\theta_y = 0$ with respect to the plane (y, z), then the same variation of C_y occurs as that shown in Fig. 11. However, the values of C_y are delaying by a phase shift equal to 90° with respect to the values shown in Fig. 11. As the crack slope increases, secondary modes of crack contact are exaggerated. These results show that the slope of the crack enforce lower range of the local flexibility variation. The previously illustrated numerical results reveal the influence of the crack breathing mechanism on the time variation of the local flexibilities. The crack breathing depends on the fracture characterizing parameters and the applied load modes. The shaft rotation complicates the breathing mechanism. For the simple loading cases

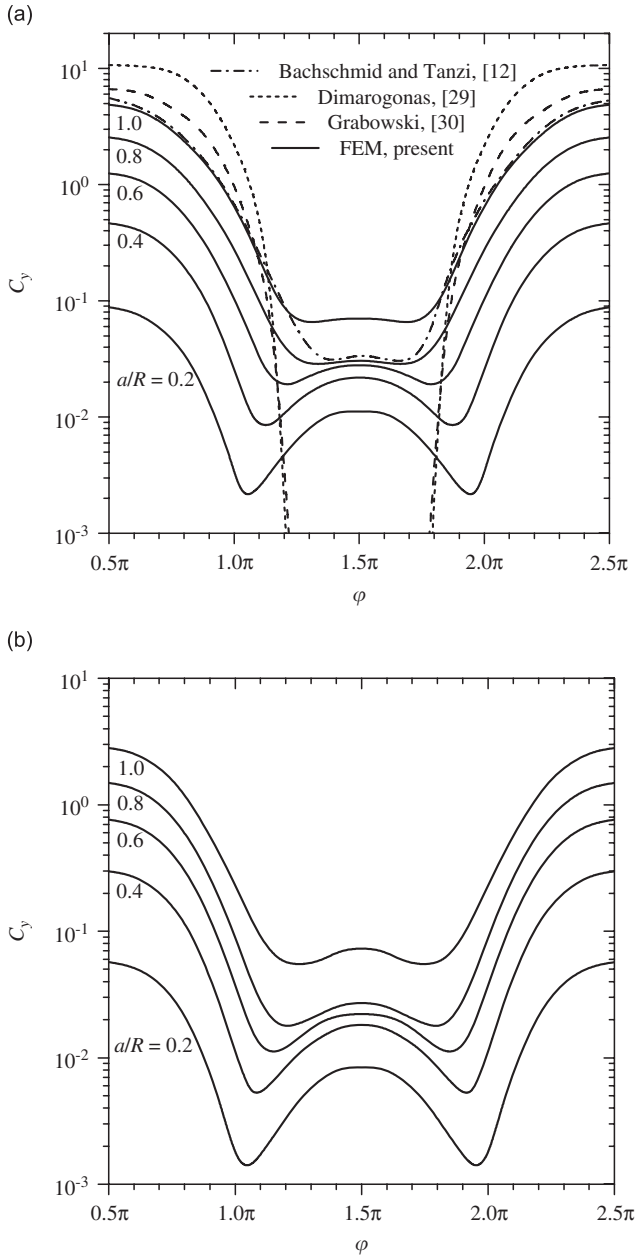

Fig. 10. Variation of bending compliance for a transversely cracked shaft as function of the load direction: (a) straight front crack and (b) curved front crack.

examined, which act independently, complicated crack breathing mechanisms are observed. The predicted crack contact implies constant flexibility coefficients or phase shifts between the varying ones, depending on the crack slope and the shape of its front. More or less, secondary contacts occur, not once per revolution, but twice per revolution. These secondary flexibilities are lower than the primary ones which occur once per revolution. This fact is known from experimental data analysis [5,11,19], but here is resolved in terms of crack contact mechanism during a variable loading. Unfortunately, these data cannot be compared directly to the present ones, due to the presence of the flywheel, the influence of its weight and the inertia terms. Careful examination of the deformation of the shaft during the loading and animation of the finite element results implies these secondary contacts, which emanate from the interaction between the temporal deformed shape of

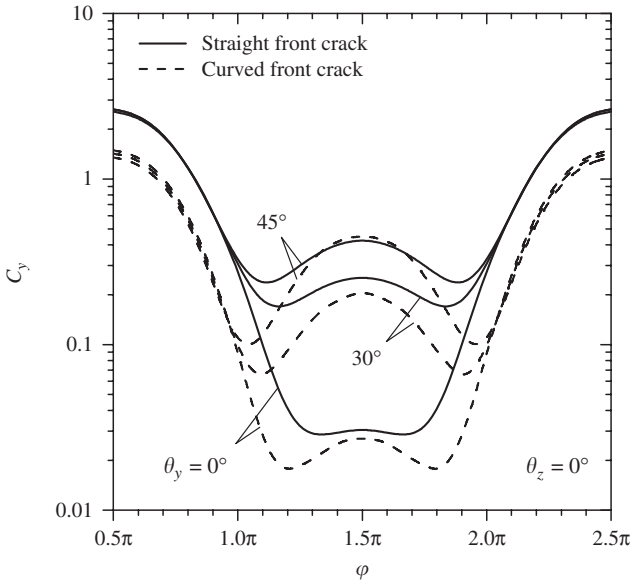

Fig. 11. Variation of bending compliance for a slant cracked shaft as function of the load direction.

the structure, the loading, and the deformation of the crack surfaces. The above parametric study reveals that the torsional local flexibility coefficient C_x is time invariant, while the bending mode local flexibility coefficients are coupled ($C_z(\varphi) = C_y(\varphi + \Delta\varphi), \Delta\varphi$, being the phase shift), and dependent on the aperture angle. If the bending is produced by the weight of the shaft itself, or general load cases are applied including shearing and axial forces, then it is expected the development of a more complicated breathing mechanism. Previous analysis gives encouraging results to adopt nonlinear finite element procedures in the dynamics of cracked rotors including temporal crack-surface interference as part of the analysis.

The proposed method is a quasi-static approach of the crack breathing mechanism applied to stationary shafts. This is the first step in the approach of the dynamic response of rotating shaft. In this case, the FEM equations representing the motion of a rotating shaft may be solved considering at each time step the quasi-static approximation just discussed. Then, the effect of inertia terms, the weight of the shaft or the externally applied loading to the crack breathing mechanism can be studied. This is a problem elaborated this time by the authors and results will be published in the near future. Authors believe that this technique may be the basis for the approximation of nonlinear dynamic response of rotors associated with crack breathing effects, for applications of non-destructive methods for crack detection.

6. Conclusions

A nonlinear finite element procedure has been presented for the simulation of the quasi-static crack breathing mechanism in rotating shafts. This procedure can predict effectively the contact evolution between the crack surfaces with the crack rotation angle. The approach concerns cantilever beamlike shafts with slant cracks, loaded in torsion or bending. At each increment of the procedure, a finite element analysis is performed and contact conditions on the crack surfaces are updated to confirm with contact criteria. Local flexibilities due to the crack are evaluated and results are presented in dimensionless form. The method yields results with reasonable accuracy as compared with experimental and theoretical results published in the literature. The evolution of portions of crack-surface contact is revealed and numerical results are illustrated showing the shape of the contact area. The crack orientation seems to play a significant role in the crack breathing mechanism. Depending on the relative crack slope with respect to the load direction, the crack remains always open or breaths. Under the open crack condition, the local flexibilities remain constant along with the shaft rotation angle. Among the crack orientation, the crack breathing behavior depends on the depth of the crack and the shape of the crack front.

References

[1] A.D. Dimarogonas, Vibration of cracked structures: a state of the art review, *Engineering Fracture Mechanics* 55 (1996) 831–857.
[2] W.G.R. Davis, I.W. Mayes, The vibrational behavior of a multi-shaft, multi-bearing system in the presence of a propagating transverse crack, *Journal of Vibration, Acoustics, Stress and Reliability in Design, Transactions of the ASME* 106 (1984) 146–153.
[3] R. Clark, W.D. Dover, L.J. Bond, The effect of crack closure on the reliability of NDT predictions of crack size, *NDT International* 20 (1987) 269–275.
[4] J. Wauer, Modelling and formulation of equations of motion for cracked rotating shafts, *International Journal of Solids and Structures* 26 (1990) 901–914.
[5] R. Gasch, A survey of the dynamic behavior of a simple rotating shaft with a transverse crack, *Journal of Sound and Vibration* 160 (1993) 313–332.
[6] T.C. Tsai, Y.Z. Wang, Vibration analysis and diagnosis of a cracked shaft, *Journal of Sound and Vibration* 192 (1996) 607–620.
[7] P.N. Saavedra, L.A. Cuitino, Vibration analysis of rotor for crack identification, *Journal of Vibration and Control* 8 (2002) 51–67.
[8] J. Zou, J. Chen, J.C. Niu, Z.M. Geng, Discussion on the local flexibility due to the crack in a cracked rotor system, *Journal of Sound and Vibration* 262 (2003) 365–369.
[9] L. Hamidi, J.B. Piaud, Modal parameters for cracked rotors: models and comparisons, *Journal of Sound and Vibration* 175 (1994) 265–278.
[10] O.N.L. Abraham, J.A. Brandon, A.M. Cohen, Remark on the determination of compliance coefficients at the crack section of a uniform beam with circular cross-section, *Journal of Sound and Vibration* 169 (1994) 570–574.
[11] A.S. Sekhar, P.B. Prasad, Dynamic analysis of a rotor system considering a slant crack in the shaft, *Journal of Sound and Vibration* 208 (1997) 457–474.
[12] N. Bachschmid, E. Tanzi, Deflections and strains in cracked shafts due to rotating loads: a numerical and experimental analysis, *International Journal of Rotating Machinery* 10 (2004) 283–291.
[13] A.K. Darpe, K. Gupta, A. Chawla, Dynamics of bowed rotor with a transverse surface crack, *Journal of Sound and Vibration* 296 (2006) 888–907.
[14] W.M. Ostachowicz, M. Krawczuk, Vibration analysis of a cracked beam, *Computers and Structures* 36 (1990) 245–250.
[15] E. Viola, L. Federici, L. Nobile, Detection of crack location using cracked beam element method for structural analysis, *Theoretical and Applied Fracture Mechanics* 36 (2001) 23–35.
[16] A.S. Bouboulas, N.K. Anifantis, Formulation of cracked beam element for analysis of fractured skeletal structures, *Engineering Structures* 30 (2008) 894–901.
[17] O.S. Jun, H.J. Eun, Modeling and vibration analysis of a simple rotor with a breathing crack, *Journal of Sound and Vibration* 155 (1992) 273–290.
[18] R.K.C. Chan, T.C. Lai, Digital simulation of a rotating shaft with a transverse crack, *Applied Mathematical Modelling* 19 (1995) 411–420.
[19] A.S. Sekhar, B.S. Prabhu, Condition monitoring of cracked rotors through transient response, *Mechanism and Machine Theory* 33 (1998) 1167–1175.
[20] Y. He, D. Guo, F. Chu, Using genetic algorithms to detect and configure shaft crack for rotor-bearing system, *Computer Methods in Applied Mechanics and Engineering* 190 (2001) 5895–5906.
[21] J-J. Sinou, A.W. Lees, The influence of cracks in rotating shafts, *Journal of Sound and Vibration* 285 (2005) 1015–1037.
[22] P. Pennacchi, N. Bachschmid, A. Vania, A model-based identification method of transverse cracks in rotating shafts suitable for industrial machines, *Mechanical Systems and Signal Processing* 20 (2006) 2112–2147.
[23] B. Andrier, E. Garbay, F. Hasnaoui, P. Massin, P. Verrier, Investigation of helix-shaped and transverse crack propagation in rotor shafts based on disk shrunk technology, *Nuclear Engineering and Design* 236 (2006) 333–349.
[24] C.S. Shin, C.Q. Cai, Experimental and finite element analyses on stress intensity factors of an elliptical surface crack in a circular shaft under tension and bending, *International Journal of Fracture* 129 (2004) 239–264.
[25] K.J. Bathe, *Finite Element Procedures*, Prentice-Hall of India, New Delhi, 1996.
[26] A.C. Chasalevris, C.A. Papadopoulos, Identification of multiple cracks in beams under bending, *Mechanical Systems and Signal Processing* 20 (2006) 1631–1673.
[27] A.J. Bush, Experimentally determined stress-intensity factors for single-edge-crack round bars loaded in bending, *Experimental Mechanics* 16 (1976) 249–257.
[28] J. Zou, J. Chen, Y.P. Pu, Wavelet time–frequency analysis of torsional vibrations in rotor system with a transverse crack, *Computers and Structures* 82 (2004) 1181–1187.
[29] A.D. Dimarogonas, C.A. Papadopoulos, Vibration of cracked shaft in bending, *Journal of Sound and Vibration* 91 (1983) 583–593.
[30] B. Grabowski, The vibrational behavior of a turbine rotor containing a transverse crack, ASME Design Engineering Technology Conference, Paper No. 79-DET-67, 1979.
[31] S. Andrieux, C. Vare, A 3D cracked beam with unilateral contact. Applications to rotors, *European Journal on Mechanics A/Solids* 21 (2002) 793–810.